Statistical modeling of transspectral processes in laser sensing of the environment. 2. Laser-induced fluorescence; model estimations

G.M. Krekov, M.M. Krekova, G.G. Matvienko, A.V. Kovshov, and A.Ya. Sukhanov

Institute of Atmospheric Optics, Siberian Branch of the Russian Academy of Sciences, Tomsk

Received December 6, 2006

Based on the algorithm of the Monte Carlo method proposed earlier for solution of nonstationary transfer equation for broadband radiation of laser-induced fluorescence (LIF), a series of calculations have been made aimed at practical purposes. As an example, we have performed quantitative analysis of the spatially resolved LIF spectra of 1H-Indole, one of the important secondary metabolites, and OPzN, a typical hazardous polycyclic aromatic hydrocarbon. We have estimated admissible distortions of the LIF spectra that would yet allow identification of the class of fluorophores to be done by the method of artificial neuron networks.

Introduction

This paper continues the discussion in Ref. 1, in which a statistical model of transfer of broadband radiation of laser-induced fluorescence (LIF) has been developed. Recently, the LIF phenomenon has determined the physical basis for the development of new methods of lidar sensing of vegetation and specific forms of organic aerosol, containing active fluorophores.

Of special interest is the problem of operative remote diagnostics of pathogenic admixtures and ecotoxicants in the near-ground atmosphere. Another one aspect of the problem is that the fluorescence spectra of pathogenic admixtures have insignificant qualitative differences from the spectra of harmless organic aerosols having close chemical nature. In this connection, the necessity appears of constructing and using quite sensitive mathematical algorithms for recognition and identification, the most popular of which in different fields of geophysics has been the method of artificial neural networks (ANN).

As shown in practice, the main factor limiting the capabilities of ANN method is the noise of active and passive origin, distorting the shape of signals to be classified. In the given case, we will concentrate on quantitative estimation of admissible distortions of the spatially resolved LIF spectra that would yet allow identification of the characteristic types of organic fluorophores to be done. In this paper, we restrict ourselves to the case of estimating the influence of active noise due to multiple scattering, occurring in the systems of fluorescence lidar sensing in a turbid atmosphere.

1. Mathematical model of the radiative transfer

The process of propagation of a short lidar signal at the wavelengths of LIF excitation will be described, as in Ref. 1, by nonstationary radiative transfer equation (RTE) through a 3D space:

$$c^{-1}\frac{\partial I(\mathbf{r},\mathbf{\Omega},t,\lambda)}{\partial t}+\mathbf{\Omega}\nabla I(\mathbf{r},\mathbf{\Omega},t,\lambda)=-\sigma(\mathbf{r},\lambda)I(\mathbf{r},\mathbf{\Omega},t,\lambda)+$$

$$+\frac{1}{4\pi}\int_{4\pi}G_{\mathrm{M}}(\mathbf{r},\mathbf{\Omega}',\mathbf{\Omega})I(\mathbf{r},\mathbf{\Omega}',t,\lambda)\,\mathrm{d}\mathbf{\Omega}'+\Phi_0(\mathbf{r},t). \quad (1)$$

Here $I(\mathbf{r},\mathbf{\Omega},t,\lambda)$ is the intensity of radiation at the wavelength λ at the point $\mathbf{r}(x,y,z)$ along the direction $\mathbf{\Omega}$, $G_{\mathrm{M}}(\lambda,\mathbf{\Omega}',\mathbf{\Omega})$ is the volume coefficient of directional elastic light scattering, $\sigma(\lambda)$ is the total extinction coefficient at the wavelength λ, that is

$$\sigma(\lambda)=\alpha(\lambda)+\sigma_{\mathrm{S}}(\lambda),$$

where

$$\alpha(\lambda)=\alpha_{\mathrm{M}}(\lambda)+\alpha_{\mathrm{F}}(\lambda),$$

α_{M} is the coefficient of absorption by the particles of the medium due to thermal dissipation, $\alpha_{\mathrm{F}}(\lambda)$ is the coefficient of absorption by fluorophores;

$$\sigma_{\mathrm{S}}(\lambda)=\sigma_{\mathrm{M}}(\lambda)+\sigma_{\mathrm{R}}(\lambda);$$

$\sigma_{\mathrm{M}}(\lambda)$ and $\sigma_{\mathrm{R}}(\lambda)$ are the coefficients of elastic and inelastic (Raman) scattering.

The external source $\Phi_0(\mathbf{r},t)$ excites fluorophores with absorption coefficient $\alpha_{\mathrm{F}}(\lambda)$ at the wavelength of laser radiation λ.

0235-6880/07/03 237-11 $02.00

The spectral intensity I_F of the subsequent emission of fluorescent light at the wavelength $\lambda' \in \Lambda$ (Λ is the region of emission spectrum) will satisfy the equation

$$c^{-1}\frac{\partial I_F(\mathbf{r},\mathbf{\Omega},\tau,\lambda')}{\partial\tau} + \mathbf{\Omega}\nabla I_F(\mathbf{r},\mathbf{\Omega},\tau,\lambda') =$$

$$= -[\sigma_M(\mathbf{r},\lambda') + \alpha(\mathbf{r},\lambda)]I(\mathbf{r},\mathbf{\Omega},t) +$$

$$+\frac{1}{4\pi}\int_{4\pi} G_M(\mathbf{r},\mathbf{\Omega}',\mathbf{\Omega})I(\mathbf{r},\mathbf{\Omega}',t)\,d\mathbf{\Omega}' + \Phi_{L_0}(\mathbf{r},\mathbf{\Omega},\lambda,\lambda'), \quad (2)$$

where

$$\Phi_{L_0}(r,\tau,\lambda,\lambda') = \frac{1}{4\pi}\phi(\lambda')\alpha_F(\lambda)q(\tau)\int_{4\pi} I(\mathbf{r},\mathbf{\Omega},\tau,\lambda)\,d\mathbf{\Omega}$$

is the function of internal LIF sources, distributed over the volume of the medium. Obviously,[2,3] it will depend on the intensity of exciting radiation, quantum efficiency (quantum yield) of the fluorescence $\phi(\lambda')$, and on the decay time $q(\tau)$.

Transformation of the transfer equation, containing the spectral dependence of the estimated functionals, into the integral form has been performed, e.g., in Refs. 4 and 5. It is shown that it preserves its canonical form of the Fredholm integral equation of the second kind:

$$f(x) = \int_X k(x',x)f(x')\,dx' + \psi(x), \quad (3)$$

where

$$X = \{(\mathbf{r},\mathbf{\Omega},t,\lambda) : \mathbf{r} \in Q \subset R^3;$$

$$\mathbf{\Omega} \in W = \{(a,b,c) \in R^3 : a^2 + b^2 + c^2 = 1\};\ t \in T, \lambda \in L\};$$

$$f(x) = \sigma(x)I(x) \quad (4)$$

has the meaning of photon collision density. Further, in equation (3)

$$k(x',x) = \frac{\Lambda(\mathbf{r}',\lambda)g(\mu,\mathbf{r}',\lambda)\exp[-\tau(\mathbf{r}',\mathbf{r},\lambda)]}{2\pi|\mathbf{r}-\mathbf{r}'|}\times$$

$$\times\delta\left(\mathbf{\Omega} - \frac{\mathbf{r}-\mathbf{r}'}{|\mathbf{r}-\mathbf{r}'|}\right)\delta\left[t' - \left(t + \frac{|\mathbf{r}'-\mathbf{r}|}{c}\right)\right], \quad (5)$$

where

$$\Lambda(\mathbf{r}',\lambda) = [\sigma_S(\mathbf{r}',\lambda) + \sigma_R(\mathbf{r}',\lambda \to \lambda')]/\sigma(\mathbf{r}',\lambda)$$

is the probability of the quanta survival;

$$g(\mu,\mathbf{r}',\lambda) = \frac{\sigma_S(\mathbf{r}',\lambda)g_M(\mu,\mathbf{r}',\lambda) + \sigma_R(\mathbf{r}',\lambda)g_R(\mu,\mathbf{r}',\lambda)}{\sigma(\mathbf{r}',\lambda)}$$

is the average weighted scattering phase function, $\mu = \cos(\vartheta)$, g_M and g_R are the scattering phase functions of elastic and inelastic scattering, normalized to unity, ϑ is the scattering angle,

$$\tau(\mathbf{r}',\mathbf{r};\lambda) = \int_0^l \sigma(\lambda,\mathbf{r},l')\,dl'$$

is the optical length of the segment $l = |\mathbf{r}' - \mathbf{r}|$, c is speed of light;

$$\psi(x) = p(\mathbf{r}_0)p(\mathbf{\Omega}_0)p(t_0)p(\lambda_0)$$

is the multiplicative density of external sources, $p(m_0)$ are the partial densities of the corresponding initial coordinates m_0. It is natural that $\int_R p(m_0)\,dm = 1$.

Based on the statistical simulation, we obtain an estimate of the intensity of backscattering of the fluorescence lidar

$$I_{i,k}(\lambda) = 1/c\Delta t_k \int_{\Delta\mathbf{r}^*}\int_{\Delta\mathbf{\Omega}_i^*}\int_{\Delta t_k} I(\mathbf{r},\mathbf{\Omega},t,\lambda)\,d\mathbf{r}d\mathbf{\Omega}dt \quad (6)$$

in the neighborhood of the given detector D. The detector is defined by the set of field-of-view angles $\Delta\mathbf{\Omega}_i^* = \sin\vartheta_d^i d\vartheta d\varphi$, the spatial volume $\Delta\mathbf{r}^* = \pi R_d^2$, and time-resolved grid $\Delta l_k = \Delta t_k c$.

The solution of the system of RTE (1) and (2) is sought under the initial and boundary conditions, corresponding to the scheme of monostatic ground-based laser radar. It is assumed that the source emits a δ-pulse in time within the direction cone $2\pi(1-\cos\varphi_i)$, where $\varphi_i = 0.2$ mrad is the full divergence angle of the source. The return signal is recorded with a receiver in the angular cones $2\pi(1-\cos\varphi_d^i)$, where φ_d^i is the set of full acceptance angles. The traditional optical characteristics of the atmosphere are, as a rule, specified by piecewise constant functions of the height h. The atmosphere is divided into n_h homogeneous layers of nonuniform height step $\Delta h_i = \Delta h_{i+1} - h_i$, $i = 1, 2, ..., n_h$. Each Δh_i layer is characterized by the assigned model values of the coefficients of optical interaction and scattering phase functions. A comprehensive description of the optical models of the atmosphere used can be found in Ref. 6. Specific features of statistical modeling of spontaneous Raman scattering have been described in Ref. 7. Below we outline the necessary aspects of the fluorescence spectroscopy.

2. Optical model of the fluorescence channel

As noted above, the main principles of constructing calculation procedures of the Monte Carlo type for solution of the problems of radiative transfer and the particular view of the generalized transition density $k(x',x)$ can be determined from analysis of the integral transfer equation (3).

In a number of cases, when complex physical conditions of the problem complicate derivation of strict analytical form of the kernel $k(x',x)$, it can be written intuitively assuming that

$$k(x',x) = P(x'_0)P(x_1)P(x_2)\ldots P(x'_n)P(x) \qquad (7)$$

is the product of the partial probability densities describing random events of consecutive interaction of the photon with scattering, absorbing, and emitting media.

The resonance and spontaneous fluorescence just belong to this class of phenomena. The main relations for the spectral intensity of the fluorescence spectrum are derived by many techniques[8]: variational method, on the basis of polarizability theory, with the help of quantum mechanics theory of perturbation, with and without taking account of the field quantization. All the methods lead to practically the same result for the simplest atomic system. In the frameworks of the traditional Kramers–Heisenberg theory,[9] for the differential scattering cross section of linearly polarized radiation with angular frequency ω, incident on an idealized nondegenerate molecule, it follows that

$$\frac{\mathrm{d}\sigma}{\mathrm{d}\Omega} = \sum_{f}^{\omega_f<\omega} \frac{\omega(\omega-\omega_f)^3}{(4\pi\varepsilon_0\hbar c^2)^2} \times$$

$$\times \left| \sum_i \left\{ \frac{\langle f|\boldsymbol{\varepsilon}_\mathrm{s}\cdot\mathbf{d}|i\rangle\langle i|\boldsymbol{\varepsilon}\cdot\mathbf{d}|0\rangle}{\omega_{i0}-\omega} + \frac{\langle f|\boldsymbol{\varepsilon}\cdot\mathbf{d}|i\rangle\langle i|\boldsymbol{\varepsilon}_\mathrm{s}\cdot\mathbf{d}|0\rangle}{\omega_{if}-\omega} \right\} \right|^2, \qquad (8)$$

where $|0\rangle$, $|i\rangle$, and $|f\rangle$ are the initial, intermediate, and final quantum states, ω_{i0} is the angular frequency of the virtual transition $0 \to i$, and ω_{if} is the angular frequency of the virtual transition $i \to f$. The angular frequency of scattered radiation is $\omega_\mathrm{s} \equiv \omega - \omega_f$. Symbols $\boldsymbol{\varepsilon}$ and $\boldsymbol{\varepsilon}_\mathrm{s}$ denote the unit vectors of the direction of polarization of the incident and scattered radiation, while $\mathbf{d}$ denotes the operator of dipole moment. Sum over all intermediate states $|i\rangle$ includes integral over the continuum of states with positive energies, i.e., over the dissociation and ionization states. Sum over all finite states $|f\rangle$ is restricted only to those states that give contributions at the observed frequency.

Formula (8) for the differential cross section includes both elastic (Rayleigh) scattering if $|f\rangle$ and $|0\rangle$ coincide (in this case, $\omega_f = 0$), and inelastic scattering (Raman effect, fluorescence), which is determined by the remaining terms in the sum over finite states $|f\rangle$. After elastic scattering event ends, the molecule (or atom) returns to the ground state $|0\rangle$.

The differential cross section of Raman scattering and fluorescence is determined by inelastic terms (i.e., $|f\rangle$, non-coincident with $|0\rangle$) of the formula (8) provided that the frequency of incident radiation ω exceeds the lowest frequency of the molecular excitation. In the general case, the amount of the frequencies ω_s in the scattered radiation is as large as the number of energy states with the frequencies ω_f not exceeding ω:

$$\frac{\mathrm{d}\sigma_{\mathrm{F,R}}}{\mathrm{d}\Omega} = \sum_{f\neq 0}^{\omega_f<\omega} \frac{\omega(\omega-\omega_f)^3}{(4\pi\varepsilon_0\hbar c^2)^2} \times$$

$$\times \left| \sum_i \left\{ \frac{(\boldsymbol{\varepsilon}_\mathrm{s}\cdot\mathbf{d}_{fi})(\boldsymbol{\varepsilon}\cdot\mathbf{d}_{i0})}{\omega_{i0}-\omega} + \frac{(\boldsymbol{\varepsilon}\cdot\mathbf{d}_{fi})(\boldsymbol{\varepsilon}_\mathrm{s}\cdot\mathbf{d}_{i0})}{\omega_{if}-\omega} \right\} \right|^2. \qquad (9)$$

In formula (9) the scalar products $\boldsymbol{\varepsilon}_\mathrm{s}\cdot\mathbf{d}_{fi}$ and $\boldsymbol{\varepsilon}\cdot\mathbf{d}_{fi}$ represent the components of dipole moment for the transition $|f\rangle \to |i\rangle$ in the direction of polarization of scattered and incident radiation ($\boldsymbol{\varepsilon}_\mathrm{s}$ and $\boldsymbol{\varepsilon}$, respectively). Analogously, $\boldsymbol{\varepsilon}_\mathrm{s}\cdot\mathbf{d}_{i0}$ and $\boldsymbol{\varepsilon}\cdot\mathbf{d}_{i0}$ are components of the dipole moment for the transition $|0\rangle \to |i\rangle$ in directions $\boldsymbol{\varepsilon}_\mathrm{s}$ and $\boldsymbol{\varepsilon}$.

When the frequency of incident radiation falls within the absorption band of a fluorophore, one term, corresponding to the transition from a certain state $|g\rangle$ to the intermediate state $|r\rangle$, may become dominating in formula (9). In addition, if the transition $g \to r$ is optically allowed, the dipole moments of these transitions are large, and so the finiteness of lifetime τ of the state $|r\rangle$ should be taken into consideration. In the absence of collisions, the width of the line of the $g \to r$ transition is determined by the radiative decay, allowing us to avoid the mathematical singularity when ω tends to the central angular frequency ω_0 of the transition $g \to r$. In this case

$$\frac{\mathrm{d}\sigma_\mathrm{F}}{\mathrm{d}\Omega} = \frac{\omega\omega_\mathrm{s}^3}{(4\pi\varepsilon_0\hbar c^2)^2} \frac{\left|(\boldsymbol{\varepsilon}_\mathrm{s}\cdot\mathbf{d}_{fr})(\boldsymbol{\varepsilon}\cdot\mathbf{d}_{rg})\right|^2}{(\omega_0-\omega)^2+(1/\tau)^2}. \qquad (10)$$

Total inelastic scattering cross section, integrated over all scattering angles and summed over all directions of polarization of light,[9] can be represented in the form

$$\sigma_{gf} = \frac{16\pi}{9} \frac{\omega\omega_\mathrm{s}^3}{(4\pi\varepsilon_0\hbar c^2)^2} \frac{|\mathbf{d}_{fr}|^2|\mathbf{d}_{rg}|^2}{(\omega_0-\omega)^2+(1/\tau)^2}. \qquad (11)$$

At the macroscopic level, the matrix elements of the dipole moment can be expressed via Einstein coefficients $\mathbf{A}_{rf}$ and $\mathbf{B}_{gr}$, characterizing the probability of spontaneous emission for the transitions $r \to f$ and the probability of absorption due to the transition $g \to r$. Following Ref. 9:

$$|\mathbf{d}_{fr}|^2 = \frac{3\pi\varepsilon_0\hbar c^3}{\omega_\mathrm{s}^3}\mathbf{A}_{rf}, \qquad (12)$$

$$|\mathbf{d}_{gr}|^2 = \frac{3\hbar^2\varepsilon_0}{\pi}\mathbf{B}_{gr}. \qquad (13)$$

Taking into account expressions (12) and (13), formula (11) takes the form

$$\sigma_{gf} = \frac{\hbar\omega\mathbf{B}_{gr}}{c\pi} \frac{\mathbf{A}_{rf}}{(\omega_0-\omega)^2+\Gamma^2}. \qquad (14)$$

As known,[10] the power of radiation, absorbed in a unity volume of a medium in the frequency interval $(\omega, \omega+\mathrm{d}\omega)$, with the neglect of induced emission is determined by:

$$P_{gr}(\omega) = \frac{\hbar\omega\mathbf{B}_{gr}N_gL(\omega)I(\omega)}{c}, \qquad (15)$$

where N_g is the number density of quantum systems which at the time t are in the $|g\rangle$ state, $L(\omega)$ is the function describing the shape of an absorption line, and $I(\omega)$ is the spectral intensity of incident radiation. Formula (15) can be written as

$$P_{gr}(\omega) = \alpha_F(\omega) N_g I(\omega), \quad (16)$$

where

$$\alpha_F(\omega) = \frac{\hbar\omega \mathbf{B}_{gr} L(\omega)}{c} \quad (17)$$

is the absorption cross section of a molecule (or an atom) in the state $|g\rangle$.

In the absence of Doppler broadening, absorption line has the classical Lorentzian shape

$$L(\omega) = \frac{1}{\pi} \frac{(1/\tau)}{(\omega_0 - \omega) + (1/\tau)^2}. \quad (18)$$

The quantum efficiency $\phi_{rf}(\omega)$ of the emission (fluorescence) due to the transition $|r\rangle \to |f\rangle$ is defined by the formula

$$\phi_{rf}(\omega) = \mathbf{A}_{rf} \tau, \quad (19)$$

i.e., the parameter $\phi_{rf}(\omega)$ expresses, actually, the probability that the quantum system in the excited state $|r\rangle$ will spontaneously emit the photon with the energy $\hbar\omega_s$.

From formulas (17) and (19) we ultimately obtain the definition of the cross section of fluorescence as a two-stage process consisting of absorption of the photon due to the transition $|g\rangle \to |r\rangle$ followed by remission due to the transition $|r\rangle \to |f\rangle$ with the probability $\phi_{rf}(\omega)$:

$$\sigma_F(\omega) = \alpha_F(\omega) \phi(\omega). \quad (20)$$

Further, because it is assumed that, in the first approximation, the spontaneous fluorescence is isotropic, the differential scattering cross section is expressed as follows:

$$\frac{d\sigma_F(\omega)}{d\Omega} = \frac{1}{4\pi} \alpha_F(\omega) Q_F, \quad (21)$$

where $Q_F = \phi(\omega)/L^F(\omega)$ is the coefficient of quenching of emitting molecule upon collisions with environment; $L^F(\omega)$ is the function describing the shape of the fluorescence spectrum.

As an independent parameter, the quenching coefficient Q_F can be determined from Stern–Volmer formula[11]:

$$Q_F = \frac{1}{1 + \Gamma_Q/\Gamma_R} = \frac{1}{1 + \sum_s \alpha_s p_s}, \quad (22)$$

where α_s is quenching coefficient of emitting molecule in collisions with components denoted by subscript s; the parameter p_s is the partial pressure of this component; and Γ_R and Γ_Q are half-widths of the radiative and collisional quenching, respectively.

3. Model estimates

The above formula (15) for the power of radiation, absorbed by the molecular system in a unit volume, includes the value N_g, which is the number density of a class of molecules capable of fluorescing within a chosen frequency interval $(\nu, \nu + d\nu)$. Precisely, this characteristic is of interest in many physicochemical, medical-biological, and ecological applications (see Ref. 1). The laboratory fluorimeters use formula (15) straightforwardly. The stand-off measurements, with frequent requirement to consider the geometric factor of observations and transmission of the optical path in the environment, employ the fluorescence laser radar equation for the energy of the backscattered signal:

$$E(\lambda, R) = E_L K_0(\lambda) T(R) \xi(R) \frac{A_0}{R^2} \frac{\sigma_F(\lambda_L, \lambda)}{4\pi} \frac{c\tau_d}{2}, \quad (23)$$

where E_L is the input energy of the laser pulse; $K_0(\lambda)$ is the transmission coefficient of the receiving system at the wavelength λ; $T(R)$ is the total transmission coefficient of the atmosphere (ocean) along the path R:

$$T(R) = \exp\left[-\int_0^R \sigma\left[(\lambda_l, R') + \sigma(\lambda, R')\right] dR'\right]; \quad (24)$$

$\xi(R)$ is the geometric shape factor of the lidar; A_0 is the area of the receiving objective, τ_d is the response time of the detector.

References 10 and 13 give detailed derivation of the lidar equation (23) and an overview of the known methods of its inversion; in addition, estimates of the possible influence of instrumental and passive atmospheric optical noise on the accuracy of solution of the lidar equation are described.

In this paper, we concentrate on the influence of active noise, accompanying the recording of laser signal; that is, we analyze the noise of multiple scattering both at the excitation wavelength λ_L and across the spectrum of the received signal of laser-induced fluorescence $\lambda \in \Lambda$ (Λ is the spectral region of recording).

The practice of such studies, performed for lidars employing the elastic and Raman scattering,[7,12,13] shows that under conditions of low visibility (smog, aerosol inversions, fog, rain, snowfall, and clouds), the backgrounds of active origin begin to play the key role in distortion of signal $E(\lambda, R)$. Rigorous numerical solution of the problem of multiple scattering of broadband fluorescent radiation is performed for the first time in the practice of atmospheric optics studies.

As an examples, we considered two model problems. One of them concerns the estimates of the transformation of LIF spectrum of octakis (pyrazol-1-yl) naphthalene (OPzN), one of the typical representatives of the polycyclic aromatic hydrocarbons (PAHs). The example has been chosen because these aromatic hydrocarbons constitute supertoxicants of the highest hazard class. At the same time, they are effectively excited by the third

harmonic of Nd:YAG laser radiation ($\lambda_l = 355$ nm), creating the physical grounds for their remote monitoring. The data on LIF spectra for OPzN were taken from Ref. 14.

In the second problem it is necessary to estimate possible distortions of the fluorescence spectrum of 1H-Indole, one of the most important secondary metabolites.[2] Indole actively manifests itself in deciduous and herbaceous plants experiencing stress being exposed to the action of some chemically aggressive substances. Moreover, Indole actively fluoresces when excited by the fourth harmonic of Nd:YAG laser radiation at $\lambda_l = 266$ nm.

Numerical analysis has been performed based on the solution of the above system of radiative transfer equations (1) and (3) by the Monte Carlo method. The solution provides the pattern of spatiotemporal and spectral LIF distribution in the region of a preset detector. The parameters of the detector and other boundary conditions, determining the region of estimation of the sought functionals, correspond to those of an actual fluorescence lidar that is being operated at the Laboratory of Lidar Methods of IAO SB RAS with the only exception that the results are extended to include those obtained for a receiver with a broad field-of-view angle. All estimates have constructed in relative units, paving grounds to believe that the data for singly scattered signals exactly correspond to the lidar signal described by the laser radar equation (23).

The really existing multiple scattering distorts the signal leading to biases in estimates of the concentration $N(R)$ of the sought fluorophore or even to its misidentification. As noted earlier,[1] the integrated quantum efficiency $\phi(\lambda)$ was taken to be constant at the level 0.03 because no exact data are available. Mean quenching time was set to be in the range 5.0–10.0 ns, which, according to numerical estimates, does not any marked effect on the coarse time grid of the signal resolution.

Let us proceed to discussion of the calculated results. Figure 1 presents estimates of spatially resolved LIF spectra as functions of the optical density of the environment: a) dense atmospheric haze, $\sigma(\lambda_l) = 0.005$ m^{-1}; and b) fog, $\sigma(\lambda_l) = 0.025$ m^{-1}.

The optical parameters of the medium, including the scattering phase function $g_M(\mu, \lambda)$ for the model of a polydisperse liquid droplet aerosol were taken from Ref. 6; values of $\sigma(\lambda_l)$ have been calculated for the excitation wavelength $\lambda_l = 325$ nm (in accordance with Ref. 14). The spectrally varying $\sigma(\lambda)$ and $g_M(\mu, \lambda)$ (not indicated in Fig. 1) were calculated in the course of simulation in the spectral region of emission $\Lambda = 350$–525 nm with the step $\Delta\lambda = 5$ nm.

The results indicate substantial distortion of the initial model LIF spectrum under conditions of fog (Fig. 1*b*), both in signal magnitude and in the shape of the spectrum, precluding its quantitative interpretation and identification. However, such conditions of experiment are extreme and, as follows from estimates obtained even for quite dense atmospheric haze (Fig. 1*a*), the LIF spectrum preserves its specific features up to sensing depth $h = 200$ m.

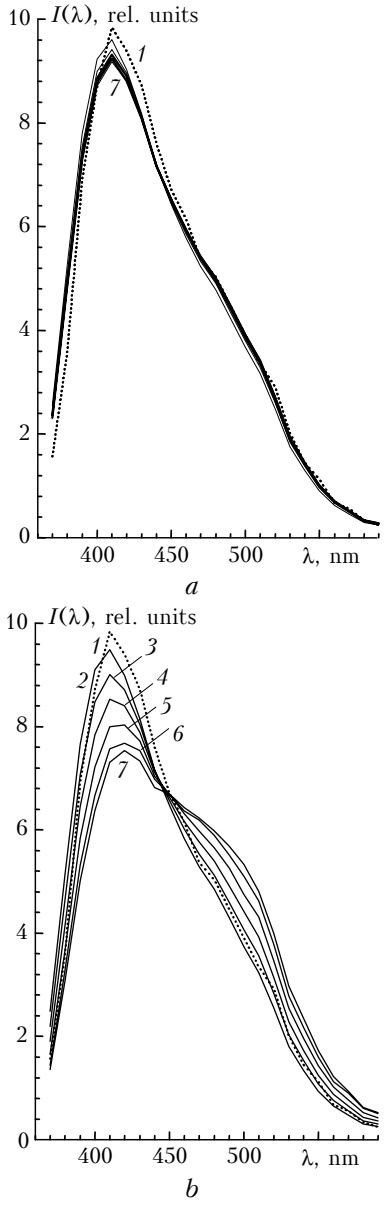

Fig. 1. Transformation of the spectrum of laser-induced fluorescence of OPzN as a function of penetration depth of laser signal and optical density of the medium: model contour (curve *1*); $h = 40$ (curve *2*); 80 (curve *3*); 120 (curve *4*); 160 (curve *5*); 180 (curve *6*); 200 m (curve *7*); $\sigma = 0.005$ m^{-1} (*a*); 0.025 m^{-1}; $\varphi_d = 1$ mrad (*b*).

The developed Monte Carlo algorithm, if necessary, can be used to study more extensively the processes of transformation of broadband radiation in a disperse medium. Figure 2 shows the spectral dependence of multiple scattering component of the total lidar signal, arrived from different depths of the medium sounded, the conditions of calculation being the same.

Obviously, in the short-wave region of the LIF spectrum, the multiple scattering contribution $F_m(\lambda)$

to the total signal $F(\lambda)$ increases faster, leading to skewness of the resulting spectrum with the increasing depth into the dense scattering medium (see Fig. 1*b*).

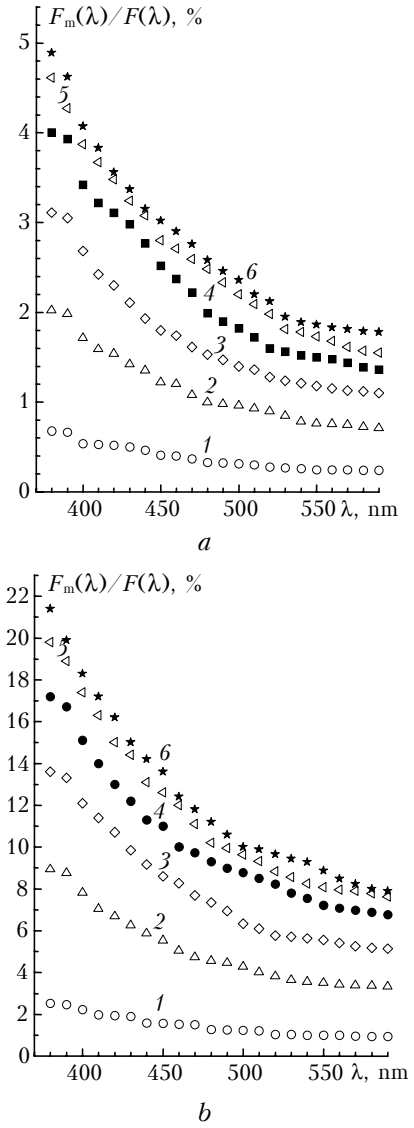

Fig. 2. Spectral dependence of multiply scattered component of the lidar signal arrived from different depths of the medium sounded: $h = 40$ (curve *1*); 80 (curve *2*); 120 (curve *3*); 160 (curve *4*); 180 (curve *5*); 200 m (curve *6*); $\sigma = 0.005$ m^{-1} (*a*); $\sigma = 0.025$ m^{-1}; $\varphi_d = 1$ mrad (*b*).

By integrating the received signal over time, these difficulties can be avoided (Fig. 3); however, the recorded signal $I(\lambda)$ will then reflect only properties of the leading edge of the medium sounded. Signal form deeper layers appears to be much weaker and thus it does not affect the integrated LIF spectrum.

At present, spectral fluorometric studies more and more actively employ wide-angle means of recording: fibers, fast video cameras, and lidars with monochromators. In this regard, by the example of LIF spectrum of Indol, we demonstrate possible consequences of such recording of spatially resolved LIF spectra (Figs. 4–6).

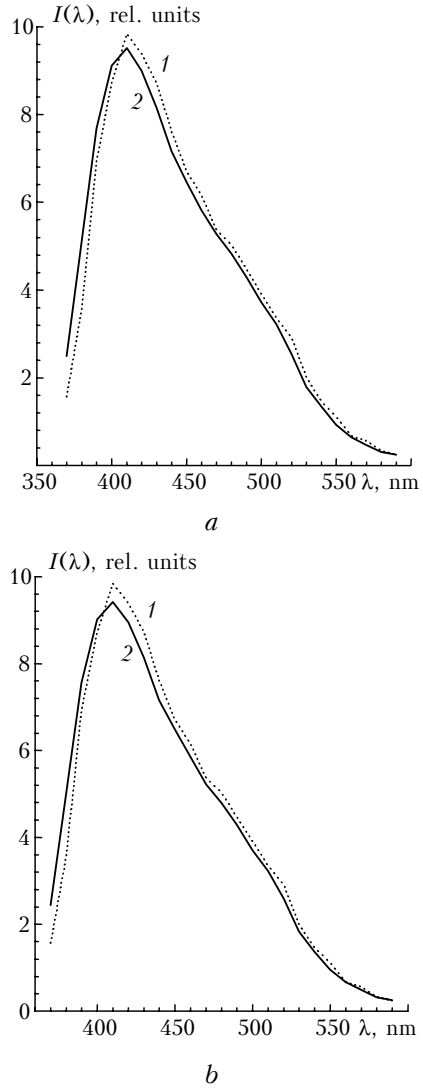

Fig. 3. Time-integrated LIF spectrum of OPzN as a function of the optical density of the medium: $\sigma = 0.005$ m^{-1} (*a*); 0.025 m^{-1} (*b*); $\varphi_d = 1$ mrad. Shown are model (curve *1*) and reconstructed spectrum (curve *2*).

Figures 4 and 5 present examples of calculated LIF spectra of Indol, excited at the wavelength $\lambda_l = 266$ nm, as functions of the detector field-of-view angle and optical density of the environment: haze (Fig. 4) and fog (Fig. 5).

Figure 4 presents spatially resolved LIF spectra, calculated for the model of a foggy haze ($\sigma = 0.005$ m^{-1}), containing isotropically distributed fluorescence centers. Transformation of the spectra reflects relative growth of the intensity of short-wave component of the fluorescence signal ("blueing of the spectrum") being a consequence of the elastic multiple scattering of fluorescence due to the increase of the detector field-of-view angle compared with its initial value $\varphi_d = 0.001$ rad.

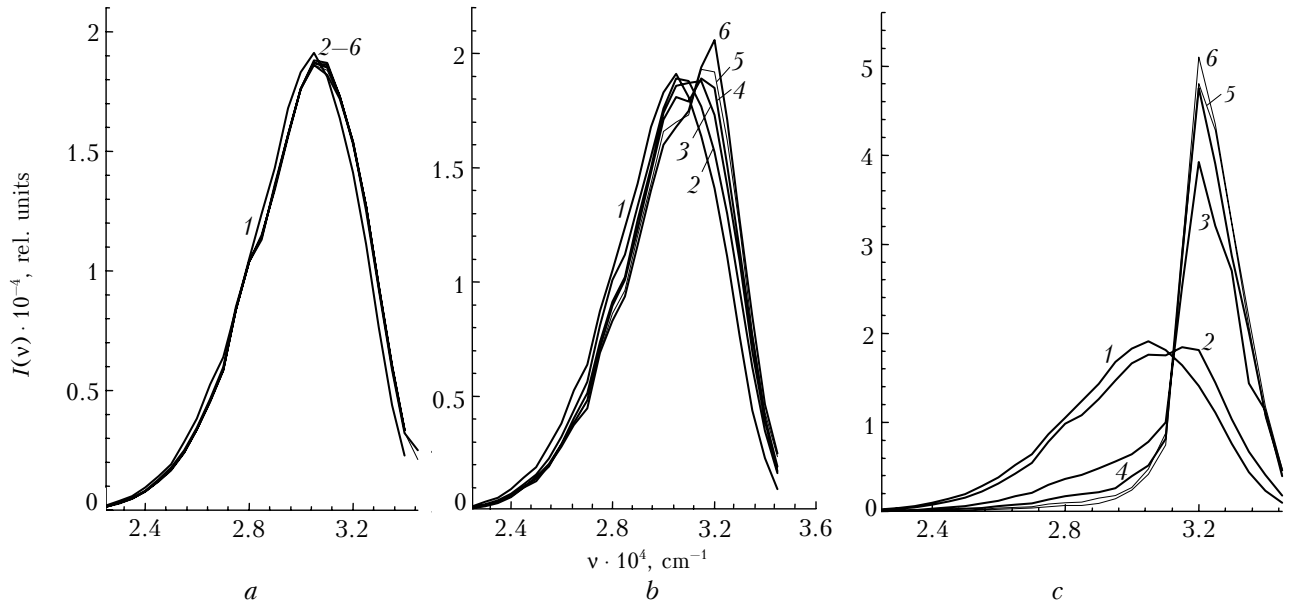

Fig. 4. Spatially resolved LIF spectra of Indol as functions of detector field-of-view angle and depth, from which the signal is returned; curves *1–6* show returns from 50, 100, 150, 200, 250, and 300 m. Extinction coefficient $\sigma = 0.005$ m^{-1}; $\varphi_d = 0.001$ (*a*), 0.01745 (*b*), and 0.0874 rad (*c*).

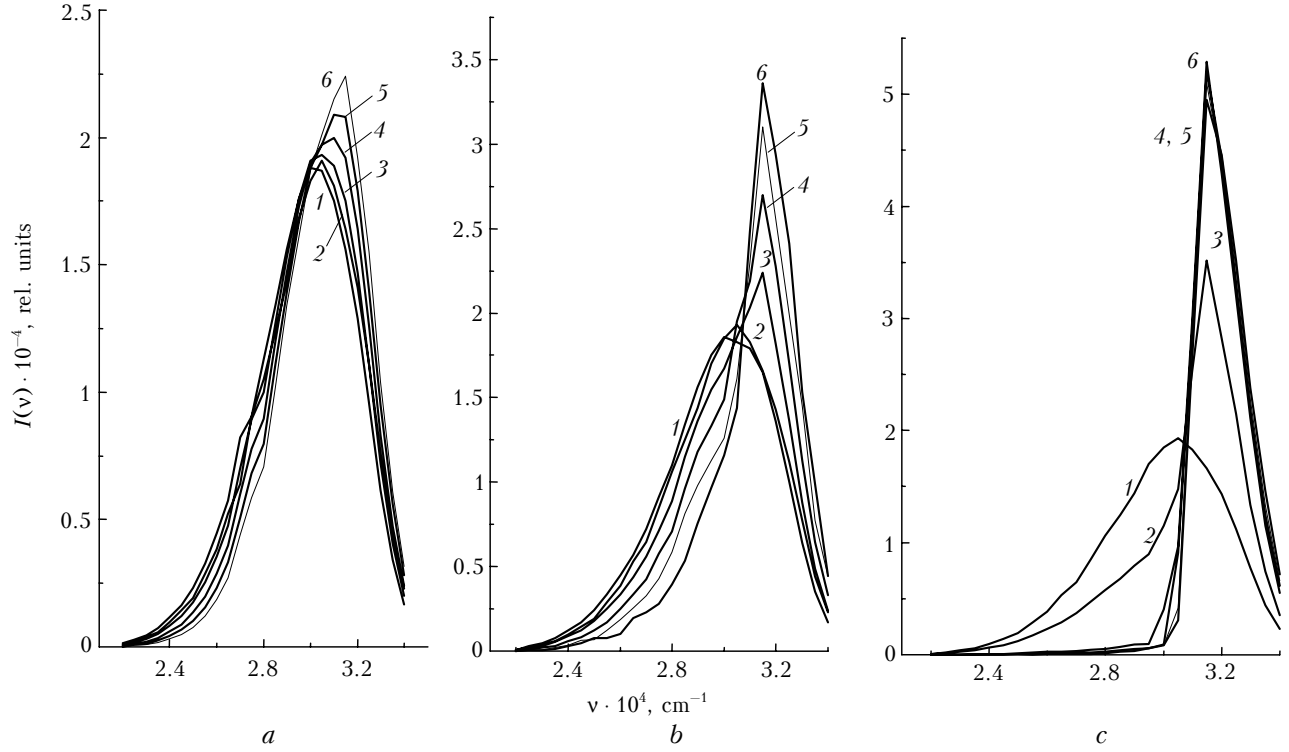

Fig. 5. Spatially resolved LIF spectra of Indol as functions of detector field-of-view angle and the depth, from which the signal comes; curves *1–6* show returns from 50, 100, 150, 200, 250, and 300 m, respectively. Extinction coefficient $\sigma = 0.02$ m^{-1}; $\varphi_d = 0.001$ (*a*), 0.01745 (*b*), and 0.0874 rad (*c*).

It should be noted that the maxima of curves, appearing in the short-wave part of the spectrum in Fig. 4*c* are practically totally caused by the multiple scattering and carry no information on the spectral behavior of LIF. This calls for care in estimating advantages of using receiving systems with wide field-of-view angles in lidar systems.

Under conditions of fog (see Fig. 5), the possibilities of acquiring a reliable signal are even more limited. Distortion of the spectrum also takes place in the small acceptance angle (see Fig. 5*a*) for the signal arriving from deeper layers of the medium. Increase of the acceptance angle leads to even larger transformation of the spectrum compared with the

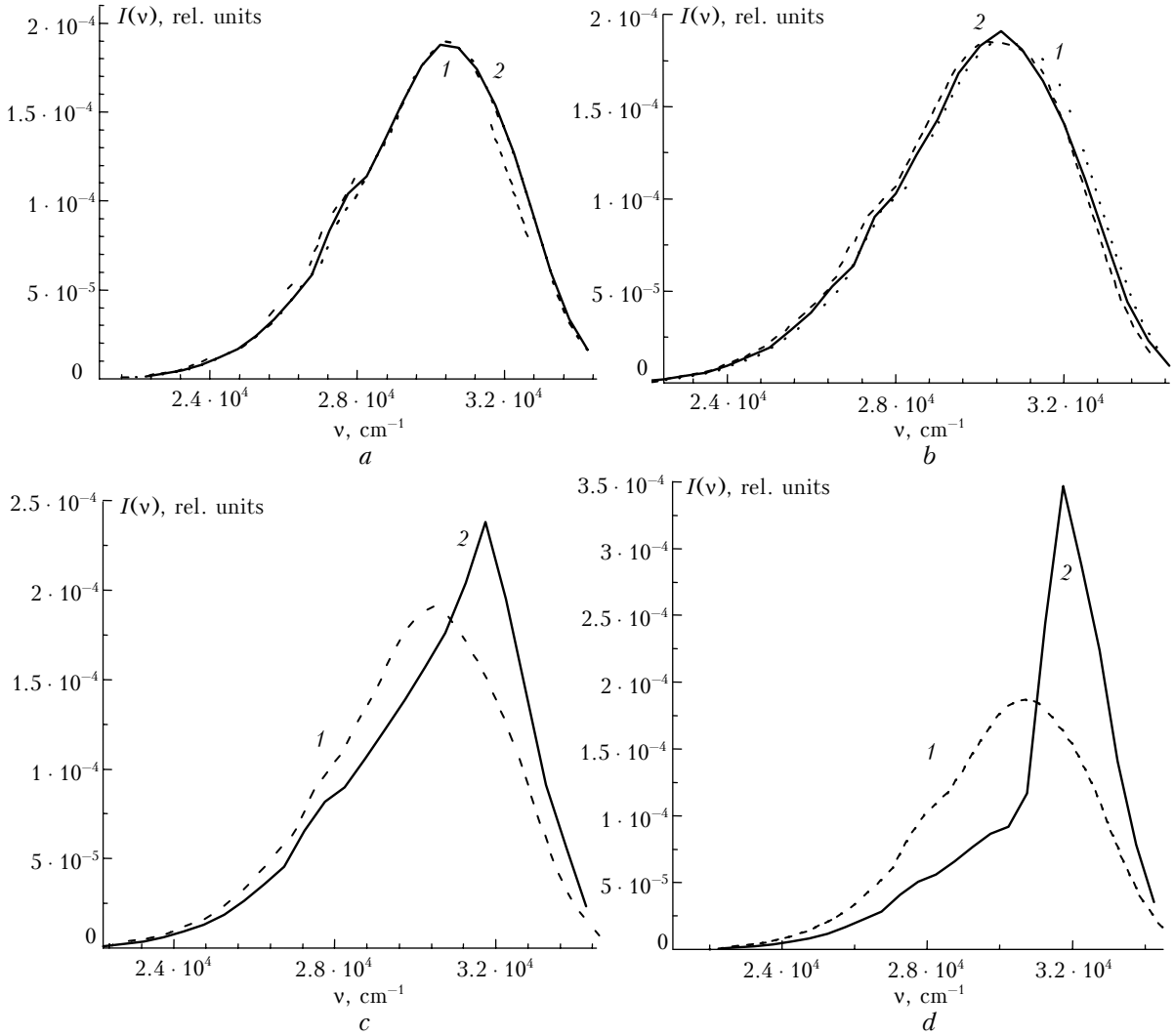

Fig. 6. Time integrated LIF spectrum of Indol as a function of the detector field-of-view angle and optical density of the environment. Shown are the model (curve *1*) and reconstructed spectrum (curve *2*). Calculations have been made for $\sigma = 0.005$ m^{-1}, $\varphi_d = 0.01745$ rad (*a*); $\sigma = 0.02$ m^{-1}, $\varphi_d = 0.01745$ rad (*b*); $\sigma = 0.005$ m^{-1}, $\varphi_d = 0.0874$ rad (*c*); and $\sigma = 0.02$ m^{-1}, $\varphi_d = 0.0874$ rad (*d*).

above-discussed case. The same conclusions as above also apply to the time integrated LIF signal (see Fig. 6). It is worthy to note the extreme distortion of the resulting LIF spectra shown in Fig. 6*d*, supporting the need in rigorous preliminary estimates of the potentialities of systems viewing in a wide angle in application to fluorometric analysis.

As concerning the further application of the mathematical apparatus of ANN, note that all spectral curves in Figs. 1–6 are reduced to the form of probability density, i.e., they are numerically normalized to unity. This also makes it possible to visually estimate the qualitative spectrum transformation independent of the penetration depth of the lidar signal.

4. Identification of LIF spectra under interference of multiple scattering

Recently, the method of artificial neural networks (ANNs)[15] has been recognized as one of the most efficient tools of image recognition. Possibilities of using the ANN method for solution of one class of problems in atmospheric optics have been demonstrated in Ref. 16.

Neural networks are a set of interrelated elements, neurons, each responding to the input effects by producing a certain output signal. Mathematically, a formal neuron can be described as follows:

$$y = \psi\left(\sum_{i=1}^{N} w_i x_i + w_0\right), \qquad (25)$$

where y is the output signal of a neuron, ψ is the activation function of the neuron, w are the weighting coefficients, N is the number of inputs, x_k are the inputs, $k = 1, 2, ..., N$, and w_0 is the threshold coefficient. Figure 7 presents a structure scheme of the formal neuron.

To provide the required functional ability, the neuron network is preliminarily trained. The training

procedure lies in that the network is given some examples, where, for each input, a certain output is put in correspondence. There can be two fundamentally different formulations of the inverse problem of remote laser diagnostics to be solved with the help of an ANN, namely the one with use of data of numerical simulation and the other one based on the database obtained directly from the experiment. In this case, the network is trained based on the "reference" results, obtained through numerical solution of the direct radiative transfer problem.

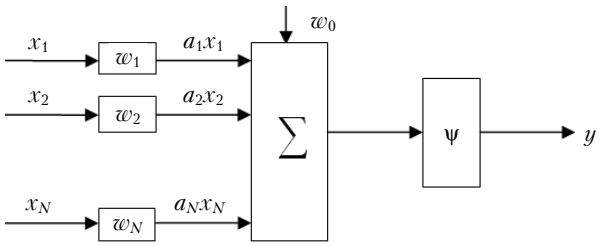

Fig. 7. Structural scheme of neuron.

One of the types of the networks, designed for image recognition, are the networks proposed by Hamming and Hopfield.[17,18] These networks mainly work with bitmaps of the images. For training of these networks, their inputs are supplied with some reference images. The difference of Hamming network from the Hopfield network lies in that the Hopfield network supplies a reference vector at its output in the case of successful recognition; whereas Hamming network indicates the reference vector number. Moreover, the number of outputs of the Hamming network equals the number of the reference vectors. The advantage of these network types is that they can recognize the input image in the case of high noise contamination, but at the same time these networks have disadvantages as well. In particular, the Hamming network can use only bitmap data presentation, while the Hopfield network has at its output the entire reference vector and it is necessary to repeatedly perform comparison with available reference vectors; moreover, the Hopfield network has low information capacity.

For recognition of the Indol spectra, we decided to use three-layer neuron network of the type of multilayer perceptron[19,20] with a single output. One-layer network is useless in this case because of the well-known limitations of these networks in classification problems due, in particular, to impossibility of separating the input images by hyperplanes of some functional dependences and train this neuron network in the case of a complex interrelations between input and output vectors. Two-layer network has less stability and requires more time for training:

$$y = \psi\left[\sum_{i=1}^{L} w_{1,i}^{3}\psi\left(\sum_{j=1}^{L} w_{i,j}^{2}\psi\left(\sum_{k=1}^{L} w_{j,k}^{1}x_k\right)\right)\right], \qquad (26)$$

where $\psi(x) = \dfrac{1}{1+\exp(-x)}$ for the last two layers and $\psi(x) = \sin(x)$ for the first layer, w^n are the weighting coefficients of the nth layer of the network, L is the number of neurons in the layer.

The values of the intensity over the spectrum are the inputs to this neural network. In the network there is only one output, which shows the possibility of recognition, this output can take real value from 0 to 1. Simultaneously, it is assumed that the spectrum is recognized when the output is larger than 0.7, and that it cannot be recognized for smaller output value. The algorithm of error back propagation is used for training the network with a cross-check by use of a test sample. The algorithm minimizes the functional of the following form:

$$E = \frac{1}{2}\sum_{l=1}^{M}\sum_{i=1}^{N}(y_i(W,X) - d_{l,i})^2 \to \min, \qquad (27)$$

where $d_{l,i}$ is the desired value, which must be provided by the input action X, $y_i(W,X)$ is the value produced by the neural network, W is the matrix of the weighting coefficients of the neurons of the network, x is the input vector, M is the number of the training examples.

Figure 8*a* presents an example when the recognition is impossible. Nonetheless, the value provided by the network is quite high because the spectrum is close to the reference one. Training sample was created by deviation of the parameters (half-width, amplitude, and center) of the Gaussian functions from the reference spectrum by a small quantity in percent of the initial values ($A_1 = 0.1 \cdot 10^{-2}$, $h_1 = 0.1 \cdot 10^{-3}$, $\sigma_1 = 0.2 \cdot 10^{-4}$, $A_2 = 0.2 \cdot 10^{-2}$, $h_2 = 0.2 \cdot 10^{-3}$, $\sigma_2 = 0.01 \cdot 10^{-2}$). It was assumed that in the case of recognition, the network must provide the value 0.95:

$$f(x) = A_1\exp\left(-\frac{(x-h_1)^2}{2\sigma_1^2}\right) + A_2\exp\left(-\frac{(x-h_2)^2}{2\sigma_2^2}\right), \qquad (28)$$

where A_1 and A_2 are the amplitudes of the Gaussian functions representing the spectrum, σ_1 and σ_2 are the half-widths, h_1 and h_2 are the centers.

For creation of the sample with the absence of recognition, we used the profiles of the spectrum with much larger percent deviation from the reference one; for these contours, the network must provide the value 0.05.

In order that the network provide a concrete values (whether the spectrum is recognized or not), the network output is complimented with a neuron possessing the threshold activation function

$$\psi(x) = \begin{cases} x > 0.7, & 1, \\ x \le 0.7, & 0. \end{cases}$$

Figure 8*b* presents an example where the recognition is possible.

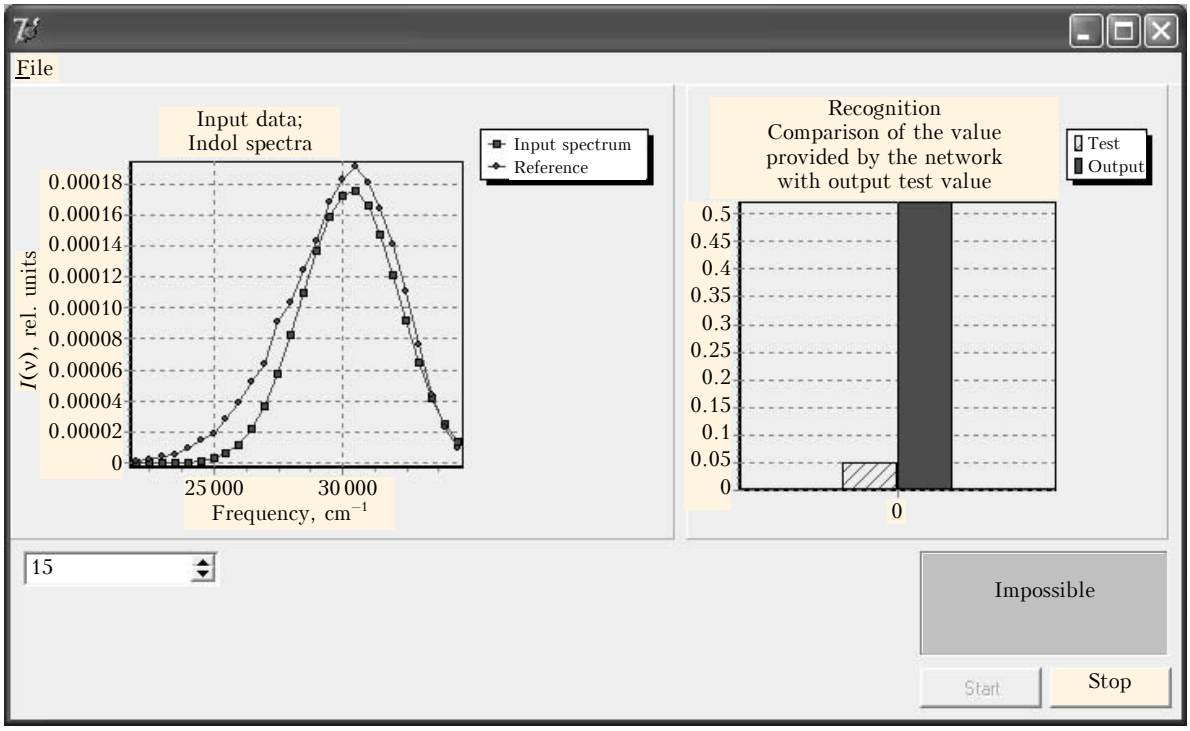

a

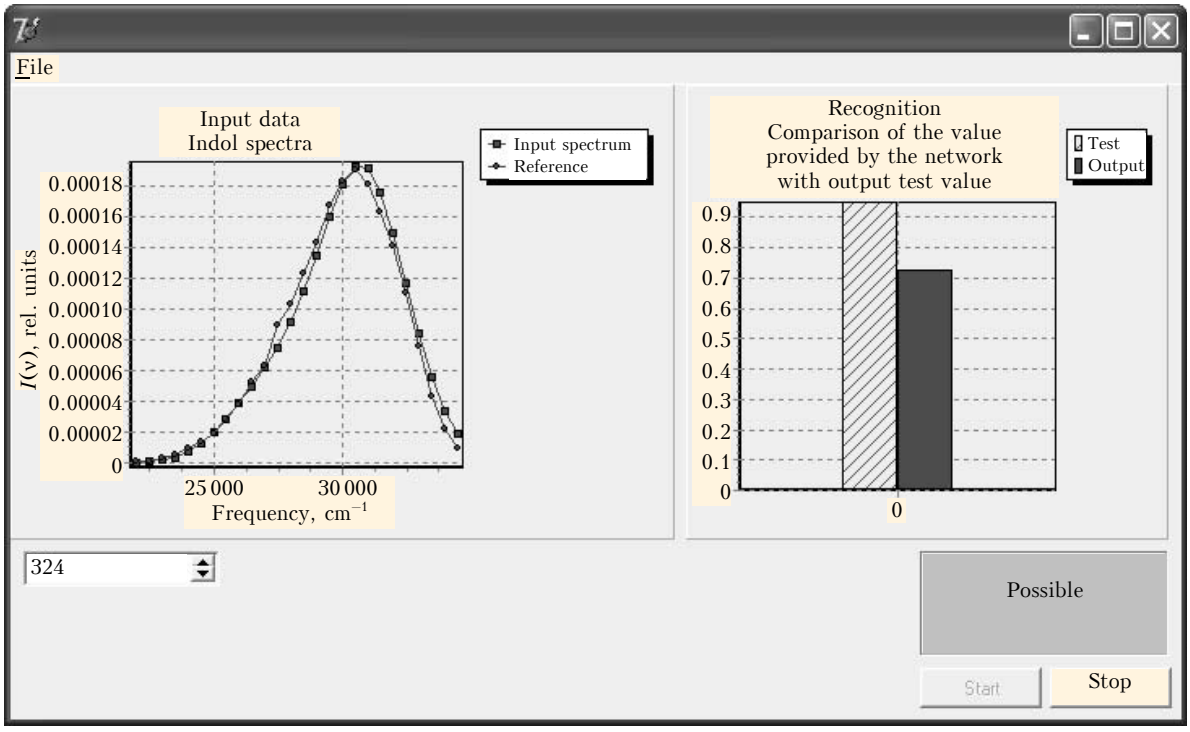

b

Fig. 8. Interface of identification of LIF spectrum: non-recognizable spectrum (*a*), recognizable Indol spectrum (*b*).

Conclusion

Based on theoretical studies presented, we proposed a new form of transfer equations or, more precisely, the system of equations describing the process of transfer of a broadband LIF in disperse media. In the framework of the Monte Carlo method, we have developed an algorithm of numerical solution of this system of RTE, allowing calculation of the spatiotemporal and spectral LIF characteristics

to be made under the boundary conditions mimicking the real experiment. We obtained numerical estimates demonstrating the efficiency of the proposed technique. The possibility of identifying the fluorescence spectra with the use of neural networks has been demonstrated. The estimates confirm the need of taking into account the background noise due to multiple scattering in case of wide field-of-view angles of the receiving optics. In the future, it is planned to incorporate the phenomena of resonance energy transfer in the case of spontaneous fluorescence in the multicomponent systems.

References

1. G.M. Krekov and M.M. Krekova, Atmos. Oceanic Opt. **20**, No. 2, 134–140 (2007).
2. J.R. Lakowicz, *Principles of Fluorescence Spectroscopy* (Plenum Press, New York – London, 1983).
3. D.Y. Paithakar, A.U. Chen, B.W. Pogue, M.S. Patterson, and E.M. Sevick-Muraca, Appl. Opt. **36**, 2260–2272 (1997).
4. Yu.E. Geints, A.A. Zemlyanov, G.M. Krekov, M.M. Krekova, and G.G. Matvienko, Atmos. Oceanic Opt. **19**, No. 10, 743–750 (2006).
5. H. Greenspan, ed., *Computing Methods in Reactor Physics* (Gordon and Breach Sci. Publ., New York – London – Paris, 1972), 372 pp.
6. V.E. Zuev and G.M. Krekov, *Optical Models of the Atmosphere* (Gidrometeoizdat, Leningrad, 1986), 256 pp.
7. G.M. Krekov and M.M. Krekova, Atmos. Oceanic Opt. **17**, No. 10, 745–752 (2004).
8. L.A. Gribov and M.A. Kovner, Zh. Prikl. Spektrosk. **45**, No. 5, 721–737 (1986).
9. R. Loudon, *Quantum Theory of Light* [Russian translation] (Mir, Moscow, 1976), 488 pp.
10. R.M. Measures, *Laser Remote Sensing* (John Wiley and Sons, New York, 1987).
11. Kh. Okabe, *Photochemistry of Small Molecules* (Mir, Moscow, 1981), 300 pp.
12. Claus Weitkamp, ed., *Lidar: Range – Resolved Optical Remote Sensing of the Atmospheric* (Springer Science + Business Media Inc., Singapore, 2005), 451 pp.
13. G.M. Krekov, S.I. Kavkyanov, and M.M. Krekova, *Interpretation of Signals of Optical Sensing of the Atmosphere* (Nauka, Novosibirsk, 1987), 185 pp.
14. C. Escolastico, M.A. Torres, M.D. Santa Maria, and R.M. Claramunt, ARKIVOC. **1**, Part 4, 612–626 (2000).
15. C.M. Bishop, *Neural Networks for Pattern Recognition.* Oxford University Press, 1995. 272 pp.
16. M.Yu. Kataev and A.Ya. Sukhanov, Atmos. Oceanic Opt. **16**, No. 12, 1020–1023 (2003).
17. J.J. Hopfield, Proc. Nat. Acad. Sci., USA **79**, 2554–2558 (1982).
18. J.J. Hopfield, Proc. Nat. Acad. Sci., USA **81**, 3088–3092 (1984).
19. D.E. Rumelhart, J.L. McClelland, and the PDP Research Group, *Parallel Distributed Processing: Explorations in the Microstructure of Cognition. Foundations* (MIT Press, Cambridge: MA, 1986), Vol. 1, 550 pp.
20. J.L. McClelland, D.E. Rumelhart, and the PDP Research Group, *Parallel Distributed Processing: Explorations in the Microstructure of Cognition. Psychological and Biological Models* (MIT Press, Cambridge: MA, 1986), Vol. 2, 632 pp.